Theoretical and experimental studies of CO2 laser evaporation of clouds

E. J. Caramana, R. B. Webster, G. P. Quigley, and R. L. Morse

Citation: Journal of Applied Physics **70**, 4601 (1991); doi: 10.1063/1.349097
View online: http://dx.doi.org/10.1063/1.349097
View Table of Contents: http://scitation.aip.org/content/aip/journal/jap/70/8?ver=pdfcov
Published by the AIP Publishing

Theoretical and experimental studies of CO_2 laser evaporation of clouds

E. J. Caramana, R. B. Webster, G. P. Quigley, and R. L. Morse[a)]
Los Alamos National Laboratory, Los Alamos, New Mexico 87545

(Received 16 January 1991; accepted for publication 11 July 1991)

A study of the effects of laser radiation on cloud drops and of the possibility of producing a clear optical channel in a cloud is presented. In order to produce a model that is appropriate to a realistic cloud with a distribution of drop sizes it is first necessary to study what happens to a single water drop subjected to laser radiation of different intensities. Various heating regimes are mapped out as a function of laser flux and fluence at the 10.6 μm wavelength. It is found that typical cloud drops can superheat until they become unstable and explode from the center. For a long laser pulse the boundary for this to occur is found to be $50(5/r)^2$ kW/cm^2, where r is the drop radius in microns. Using these results a model that is spatially one-dimensional through the cloud is constructed for a distribution of drop sizes. Laser beam intensity as the light penetrates a cloud is calculated from Mie scattering and absorption cross sections for a beam diameter that is small in the sense that light scattered once is assumed lost. The internal temperature distribution of the drops is calculated and a phenomenological drop explosion model is given for drops that reach the unstable 305 °C spinodal temperature at their center. Energy and water mass content are conserved as the cloud background is modified in an average sense by drop evaporation or recondensation. Recondensation is treated in the diffusion regime according to the Kohler model, with vapor pressure over a drop modified by surface tension and dissolved nonwater content. Comparison with experimental data for a laboratory produced cloud is given and good agreement, particularly with respect to the predicted onset of drop explosion, is found. Results are also presented for hypothetical cloud conditions and laser intensities. The possibility of clearing a thin cloud with low fluence to the 3.8 μm is considered, as well as the passive evaporation of melted ice crystal clouds.

I. INTRODUCTION

By clearing an optical channel into or through a cloud with a pulsed laser beam, access can be gained for optical diagnostics to measure internal properties of the cloud. For example, from the velocity of penetration of the beam head and the intensity of the backscatter of the clearing beam the condensed water content and mean drop size could be estimated. With the backscatter of one or more concurrent probe beams at wavelengths substantially different from the clearing beam, additional features of the drop distribution could be determined. For measurements requiring back lighting of a cleared channel through a cloud the beam could be directed toward a bright celestial object. Motion of the sides of the cleared channel would indicate turbulent wind velocities along the channel. For these diagnostic purposes it would be necessary to be able to predict from a theoretical model the details of the clearing of a channel and subsequent recondensation in the channel under the various possible cloud conditions.

In this paper we present a detailed study of vaporization, recondensation, and other effects of CO_2 laser radiation at the 10.6-μm wavelength on individual cloud water drops as well as on a cloud consisting of a size distribution of water drops. The CO_2 laser is chosen because it is efficient, produces radiation in the region where liquid water absorbs relatively well, and is not strongly absorbed by water vapor. This paper is organized as follows.

In Sec. II the single drop model is explained in detail. This includes thermal diffusion through the drop interior and energy balance at the drop surface. Several different boundary conditions for the temperature at the drop surface are derived. These delineate the various heating regimes. It is found that the drops can superheat in the interior for a modest incident laser flux (50 kW/cm^2 for a 5-μm radius drop) to a point where the unstable spinodal temperature of 305 °C is reached in the center. A high-pressure ($\sim$220 atm) region is then spontaneously produced that explodes the drop from the center outward. Evaporation at the drop surface before this time is negligible. The phenomenology for cloud drops to reach the spinodal temperature is developed as a function of incident laser flux, fluence, and drop size. In addition, we delineate for a given constant laser flux versus initial drop size the various regimes of relevance for vaporization of water drops by a CO_2 laser, assuming volume absorption. Because internal explosion occurs for a relatively low laser flux, other regimes involving rapid surface ablation at a much higher laser flux are not accessible before internal droplet explosion occurs. For a high CO_2 laser flux (>1 MW/cm^2) all cloud drops from 1 μm in radius and larger will explode.

In Sec. III a multiple drop cloud model is constructed using the results of the single drop model. This includes a heuristic model for drop explosion, and a recondensation model that treats the basic physics of natural cloud drop formation. The drop size distribution function is dis-

[a)]Presently at University of Arizona, Tucson, AZ 85721.

 0021-8979/91/084601-16$03.00

cretized with respect to initial drop size and the amount and type of nonwater constitution. All quantities, including background temperature and pressure, can depend on the vertical z coordinate through the cloud. The Kohler phenomenology is developed and extended to include a constant laser flux. This allows a simple description in terms of equilibrium drop sizes of vaporization and recondensation. It is seen that if the supersaturation level of the cloud environment is increased sufficiently, all initial cloud drops will grow after the laser is turned off. A number of points, such as the importance of ambient temperature and drop solute concentration on recondensation, are considered. A dimensionless parameter giving the relative importance of air thermal diffusion and vapor diffusion to the recondensation process is derived.

Section IV presents a comparison with experimental results obtained in the laboratory. This is done by monitoring the transmission and scattering of a passive visible probe laser as a function of time into the CO_2 clearing pulse. An explosion event is indicated by a sharp decrease in transmission and an increase in scattering of the probe beam. Both the flux and total fluence to the onset of the explosion event is compared to the theoretical calculations. Good agreement is found. Recondensation rates are predicted to be enhanced by at least a hundred for the parameters considered due to the increase in nucleation sites resulting from droplet shattering. Also considered is the possibility of using a 10.6-μm laser to clear a thin cloud (thickness of approximately one e-folding to the initial 10.6-μm wavelength) for propagation of the 3.8-μm wavelength radiation. This can be accomplished with an order of magnitude less fluence than previously believed by shattering drops so that the Rayleigh regime is achieved at 3.8 μm. Finally, the passive evaporation of laser melted ice crystals is considered. In the Appendix we briefly describe how the multiple drop cloud model in both the low and high laser flux regimes is numerically implemented.

II. SINGLE DROP MODEL

The equations for energy conservation at the surface of a water drop of radius $r_d(t)$ and thermal diffusion across the drop are given by

$$\rho_w L r_d^2 \frac{dr_d}{dt} = \kappa_a r_d (T_s - T_a) + \kappa_w r_d^2 \left.\frac{\partial T_d}{\partial r}\right|_{r_d -}, \tag{1}$$

$$\rho_w c_w \frac{\partial T_d}{\partial t} = p_l + \frac{\kappa_w}{r^2}\frac{\partial}{\partial r} r^2 \frac{\partial T_d}{\partial r}, \tag{2}$$

respectively, in the spherically symmetric approximation. Here ρ_w is the mass density of water, L is the latent heat of vaporization, and c_w is the specific heat; κ_a and κ_w are the thermal conductivities of air and water, respectively. $T_d(r,t)$ is the internal drop temperature distribution. T_s and T_a are the temperatures of the drop surface and of the air far from the drop; finally, $p_l(t)$ is the laser absorption source term, r is the radial coordinate, and t is time. The first equation says that the energy that goes into evaporation of the drop is equal to minus the thermal conduction to the air plus the thermal diffusive flux at the drop surface. Thus it is seen immediately that there must be a temperature gradient across the drop for any evaporation to occur. The second equation expresses thermal diffusion in the drop interior with a spatially uniform heating rate, p_l, that is calculated from Mie theory and depends only on laser flux and total drop radius.[1,2] Since typical cloud drops are less than 10 μm in radius it is valid to treat the energy deposition within a single drop as uniform. This greatly simplifies the single drop heating model given above, making it one-dimensional. The first equation essentially determines the time evolution of the drop radius $r_d(t)$. For the model to be complete the second equation, which determines the internal drop temperature profile $T_d(r,t)$, must be supplemented by a boundary condition on the temperature at the drop surface $T_d[r_d(t),t] \equiv T_s(t)$. The proper specification of this boundary condition is given in the detailed discussion below. It is important to note that Eqs. (1) and (2) are defined on the variable domain $[0 \leqslant r \leqslant r_d(t)]$. To simplify the solution Eqs. (1) and (2) are transformed to a new spatial representation based on the coordinate $x \equiv r/r_d(t)$, which is fixed in time and has unit domain. This transformation introduces into Eq. (2) an advective term $(1/r_d)(dr_d/dt)x(\partial T_d/\partial x)$ since the time derivative in Eq. (2) is now with respect to constant x rather than constant r.

A. Boundary conditions and drop heating regimes

In situations of intense heating the drop warms quickly, then the simplest boundary condition that can be specified for Eq. (2) is to set the drop surface temperature equal to the boiling point of water $T_s = T_b$ at the local atmospheric pressure. Then one also initializes $T_d(r,0) = T_b$ and the superheating of the drop in the interior can be followed. In this manner the conditions under which the unstable 305° temperature is reached in the droplet center can be determined. Droplet explosion is assumed to occur as soon as this temperature is reached. This scenario assumes a laser power sufficient to heat the drop to boiling and that once boiling is reached that the surface ablates rapidly enough that the surface temperature does not rise significantly above boiling. This is actually a good description for high laser powers, but to examine the validity of heating regimes particle balance at the drop surface must be considered.[3]

The mass flux Γ of water molecules at the drop surface per unit area is given by

$$\Gamma = Be^{-LM_w/RT_s} - \alpha\rho_v(r_d)v_n, \tag{3a}$$

$$v_n = \sqrt{RT_s/2\pi M_w}, \tag{3b}$$

where R is the gas constant and $M_w = 18$ is the molecular weight of water. Here the first term gives the rate of emission of water molecules from the drop surface. This is the usual Boltzmann factor. Note the strong dependence on the latent heat of vaporization L and the surface temperature T_s. The second term in Eq. (3a) gives the rate of adsorption of water molecules from outside the drop, where α is the sticking coefficient (close to unity for water

vapor; however, our results are insensitive to its precise value), v_n is the average velocity normal to the surface (1/4 of the mean thermal speed), and $\rho_v(r_d)$ is the water vapor density at the drop surface. In Eq. (3b) we have assumed that the mean free path for a water molecule just outside the drop is small compared to the temperature gradient scale length. The coefficient B in Eq. (3a) can be found by using the thermodynamic equilibrium value for $\rho_v(r_d)$, whence the flux $\Gamma = 0$. This can be calculated by means of the Clausius–Clapeyron equation and the ideal gas law. These are given by

$$p_{sv}(T_s) = p_r e^{(LM_w/R)(1/T_r - 1/T_s)}, \tag{4}$$

$$\rho_s(T_s) = \frac{M_w}{RT_s} p_{sv}. \tag{5}$$

In Eq. (4) p_r, T_r are reference values of pressure and temperature and $p_{sv}(T_s)$ is the equilibrium pressure of water vapor over a flat surface at the temperature T_s. (Modifications due to curvature and dissolved solute will be given later.) Thus, using Eqs. (4) and (5) in Eq. (3a) and setting $\Gamma = 0$ yields $B = (\alpha/2\pi v_n) p_r \exp(LM_w/RT_r)$. Knowing B, the expression for the flux Γ of water vapor emitted at the drop surface takes the simple and somewhat intuitive form

$$\Gamma = \alpha v_n [\rho_s(T_s) - \rho_v(r_d)]. \tag{6}$$

From mass conservation we have

$$\frac{dr_d}{dt} = -\frac{\Gamma}{\rho_w}. \tag{7}$$

By combining Eqs. (1), (6), and (7) we obtain

$$\frac{\kappa_a(T_s - T_a)}{Lr_d} + \frac{\kappa_w}{L}\frac{\partial T}{\partial r}\bigg|_{r_d -} + \alpha v_n[\rho_s(T_s) - \rho_v(r_d)] = 0, \tag{8}$$

which gives the desired expression for the boundary condition $T_s(t)$ if we know $\rho_v(r_d)$. The determination of $\rho_v(r_d)$ not only completes the problem but also defines the various evaporation regimes. Simplest is the diffusion regime, given by $\nabla^2 \rho_v = 0$ exterior to the drop with the boundary condition $\Gamma = -D\nabla\rho_v|_{r_d +}$, where $D \approx 0.22$ cm^2/s is the diffusion coefficient for water vapor. For spherical symmetry the solution has the form $\rho_v = a/r + \rho_{v\infty}$, whence $\Gamma = Da/r_d^2$. Thus using Eq. (6) the water vapor density outside the drop is given by

$$\rho_v(r) = \alpha \frac{[\rho_s(T_s) - \rho_{v\infty}] r_d}{[(D/r_d v_n) + \alpha] r} + \rho_{v\infty}$$

$$\approx [\rho_s(T_s) - \rho_{v\infty}]\left(1 - \frac{D}{r_d v_n \alpha}\right)\frac{r_d}{r} + \rho_{v\infty}. \tag{9}$$

The quantity $D/(r_d v_n)$ appears as the ratio of two velocities and for $T_s = 300$ K is a small number for $r_d > 0.15\,\mu$m. Since cloud drops are larger than this, and for α not too much smaller than one, the expression for Γ, using the approximate form of Eq. (9) in Eq. (6), in the diffusion regime assumes the simple form

$$\Gamma = \frac{D}{r_d}[\rho_s(T_s) - \rho_{v\infty}]. \tag{10}$$

Notice that the sticking coefficient no longer appears in Eq. (10).

To obtain the limit where vapor convection in isobaric flow from the drop surface first becomes important we need to consider two fluid flow.[4] The equations for the diffusion of water vapor through air outside of a vaporizing spherical liquid drop ($r \geqslant r_d$) can be written in the steady state approximation as

$$\left(\rho_v V + \frac{D(\rho_v \nabla\rho_a - \rho_a \nabla\rho_v)}{(\rho_v + \rho_a)}\right) 4\pi r^2 = -4\pi r_d^2 \rho_w \frac{dr_d}{dt}, \tag{11a}$$

$$\rho_a V - \frac{D(\rho_v \nabla\rho_a - \rho_a \nabla\rho_v)}{(\rho_v + \rho_a)} = 0. \tag{11b}$$

In these equations $\rho_a(r,t)$ and $\rho_v(r,t)$ are the air and water vapor mass densities outside the drop, V is the velocity of the composite fluid $\rho_v + \rho_a$, and the source term on the right-hand side of Eq. (11a) is the rate of drop mass vaporization. Since we have only two equations but three unknowns (ρ_a, ρ_v, V) another assumption must be made to complete the model. If we consider the air and water vapor outside the drop to be isothermal as well as isobaric so that only interspecies diffusion is important then

$$\rho_v + \rho_a = \rho_{a\infty} + \rho_{v\infty}, \tag{12}$$

where $\rho_{a\infty}$ and $\rho_{v\infty}$ are the air and water vapor mass densities far from the drop. Then Eqs. (11) become

$$\frac{\rho_w[\rho_v(r) - \rho_{a\infty} - \rho_{v\infty}]}{(\rho_{a\infty} + \rho_{v\infty})}\frac{r_d^2}{r^2}\frac{dr_d}{dt} + D\frac{\partial \rho_v}{\partial r} = 0. \tag{13}$$

In the limit $\rho_v \ll \rho_{a\infty}$ this equation, by using the divergence theorem in spherical geometry, yields the diffusion approximation just given. The solution of Eq. (13) is seen to be

$$\rho_v(r) = (\rho_{a\infty} + \rho_{v\infty}) - \rho_{a\infty} \exp\left(\frac{\rho_w r_d^2 (dr_d/dt)}{D(\rho_{a\infty} + \rho_{v\infty}) r}\right). \tag{14}$$

Let $A \equiv \rho_w r_d^2 (dr_d/dt)/[Dr_d(\rho_{a\infty} + \rho_{v\infty})]$, then $A \approx 1$ defines the boundary where convective effects become important [$\exp(A) \approx 1 + A$ gives the diffusion regime result]. Neglecting $\rho_{v\infty}$, the dimensionless parameter A can be interpreted as the ratio of the water vapor mass production rate

$$\frac{\rho_w}{r_d}\frac{dr_d}{dt}$$

to the characteristic mass diffusion rate of vapor across the drop radius

$$\frac{\rho_{a\infty} D}{r_d^2}.$$

When water vapor is produced slowly ($A < 1$) it is able to diffuse into the air without modifying the air density profile

significantly. When water vapor is produced quickly ($A > 1$) it pushes air away from the drop surface and convection is important.

A more realistic closure of Eqs. (11) is to let the temperature away from the drop also follow a steady state diffusion law whose solution is given by

$$T(r) = (T_s - T_a)\frac{r_d}{r} + T_a, \tag{15}$$

and simply keep the isobaric constraint. Then the solution for $\rho_v(r)$ analogous to that given by Eq. (14) becomes

$$\rho_v(r) = \frac{r}{(T_s - T_a)r_d + T_a r}\left\{p_\infty + (T_a\rho_{v\infty} - p_\infty) \times \exp\left[\frac{r_d^2\rho_w}{Dp_\infty}\frac{dr_d}{dt}\left(\frac{r_d(T_s - T_a)}{2r^2} + \frac{T_a}{r}\right)\right]\right\}. \tag{16}$$

B. Numerical solutions of single drop model

The numerical solution of our model is quite straightforward. First Eq. (2), which determines the internal drop temperature profile, is implicitly differenced on a uniform spatial grid with respect to the fixed independent variable x previously defined. Equation (1) is solved to obtain the new drop radius. Both this equation and the equations that give the drop surface temperature T_s must be iterated along with Eq. (2) until convergence is reached, defining the end of a timestep. To obtain T_s we use either of Eqs. (9), (14), or (16) for $\rho_v(r_d)$ in Eq. (8) giving an implicit relation for T_s. Then Eq. (1) is used in this expression to eliminate the explicit appearance of dr_d/dt. Newton iteration is used to obtain a converged T_s. This depends crucially on the correct temperature gradient inside the drop surface $\partial T/\partial r|_{r_d-}$. Consistency of the solution inside and outside of the drop surface is checked by seeing that the same value for dr_d/dt is obtained from either Eq. (1) (inner solution) or from Eqs. (6) and (7) (outer solution). It is important to note that the combination of Eq. (8) with either Eq. (14) or Eq. (16) becomes singular when the vapor pressure over the surface of a drop at temperature T_s, as predicted by Eqs. (4) and (5), becomes greater than atmospheric pressure. This is because to close Eqs. (11) to obtain Eq. (14) or Eq. (16) the isobaric assumption was made. This breaks down when hydrodynamic effects become important, that is, when Eqs. (11) which describe steady-state two fluid flow driven by a nearly constant source term are not valid. Equation (9), which describes the diffusion regime, is physically invalid before the convection regime is reached but it does not become singular for any drop surface vapor density or pressure. Equation (9) is still useful, even in this high-pressure regime, because it places an upper bound on the value of the drop surface temperature that can be obtained for any given laser power. This is because predicted surface temperatures above the boiling point result, from Eq. (4), in saturated equilibrium water vapor pressures above the ambient atmospheric pressure. Since this actually gives rise to hydrodynamic flow one would expect the physical drop surface temperature to be less than that resulting from Eq. (9).

As has been alluded to previously, drops whose central temperature reaches about 305 °C will spontaneously form water vapor at about 220 atm pressure and explode from the inside.[5] This process, "spinodal decomposition," can be understood simply from the nonmonotonic isotherms of the Van der Waals equation of state on a pressure versus volume ($P - V$) diagram.[6] If a liquid is heated fast enough and there are no readily available vapor nucleation sites (as for a water drop suspended in air) it can become superheated above its boiling point for the given external gas pressure. Thus it evolves across the Van der Waals loops (it is not an isotherm when heating) until it reaches the spinodal curve. This curve is defined by the locus of points on all of the isotherms on a ($P - V$) diagram where $dP/dV|_T$ becomes positive (thermodynamically unstable). For about 1 atm external pressure this temperature is $\approx$ 305 °C at which the equilibrium vapor pressure is about 220 atm. The spontaneous liquid to vapor phase transition thus occurs at this pressure causing an explosion.

In Fig. 1 is shown numerical results of the model for a water drop with a 5-μm initial radius and a laser power of 50 kW/cm^2. Figure 1(a) gives a series of profiles of internal temperature versus radius for the first 30 μs. Here the diffusion regime boundary condition for the drop surface temperature is used. The initial drop temperature is 0 °C and the drop is initially in equilibrium with water vapor at this temperature. The solid, dotted, and dashed curves are at 10, 20, and 30 μs, respectively, after the laser is turned on. This sequence illustrates the initial fast heating phase. Note that by the time the unstable 305 °C temperature has been reached in the center the radius is still over 90% of its initial value. The temperature at the edge of the drop is 180 °C which, as previously noted, is an upper bound on this quantity and corresponds to an equilibrium pressure of $\sim$10 atm. Although this would result in a rapid vapor expansion and subsequent cooling, the rate of drop vaporization, as seen from Eq. (1), depends on $\partial T/\partial r|_{r_d-}$ and is thus not very sensitive to the value of T_s or what occurs outside the drop surface. This can be seen from Fig. (1b) which gives results for the same parameters except that the drop surface temperature is held fixed in time at the boiling point (100 °C) and the initial drop temperature is also set at this value. The solid, dotted, and dashed curves are the temperature versus radius at 10, 20, and 30 μs, respectively, after the laser is turned on. We see that if a drop is heated to the unstable temperature in its center where explosion occurs it still has a substantial temperature gradient across its radius. Thus it cannot just become a single large vapor bubble since sufficient stored internal energy relative to the value of the latent heat of vaporization at the boiling point does not exist.

In Fig. 1(c) is shown the temperature at the drop center versus time assuming no explosion occurs for the case shown in Fig. 1(b). Note that there is a rapid increase followed by a slow decrease. Since, as seen from Fig. 1(c), the 305 °C center temperature is just reached for the 50 kW/cm^2 power level we conclude that if a drop explodes at all for a given laser flux it will do so before it has evaporated substantially. The slow decrease in central drop tem

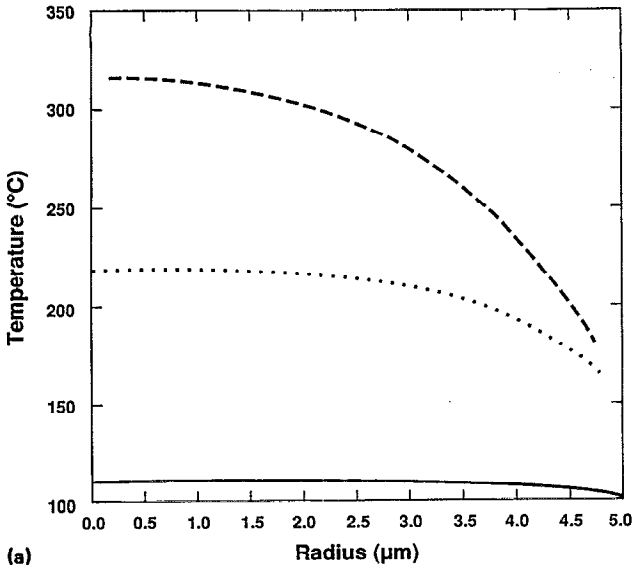

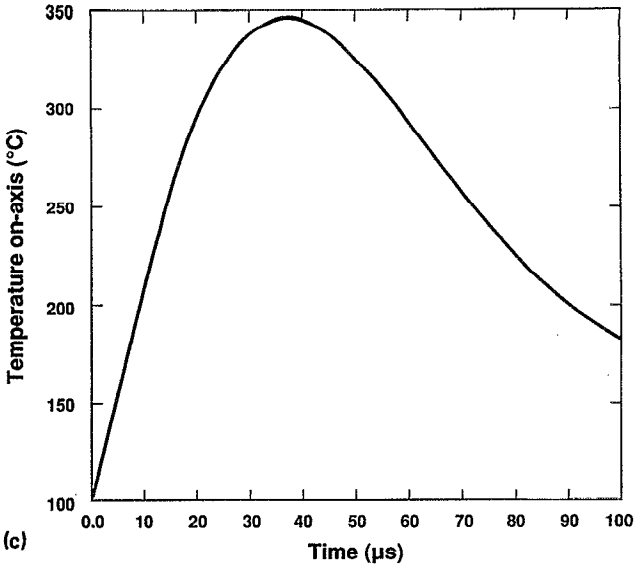

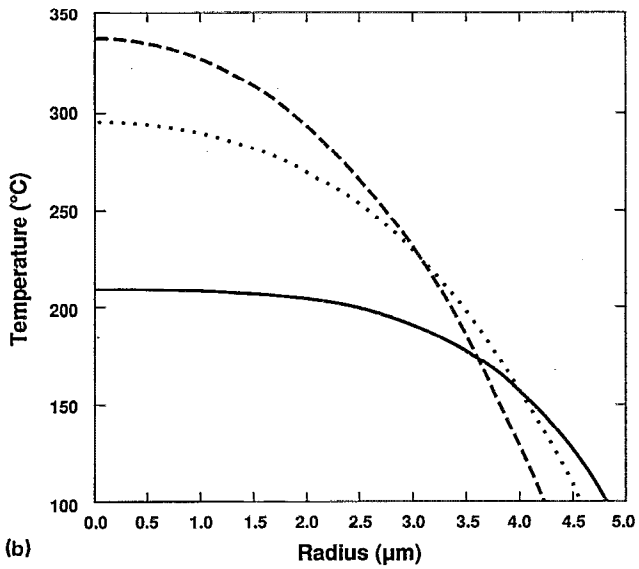

FIG. 1. Results for a 50 kW/cm^2 CO_2 laser incident on a drop with an initial drop radius of 5 μm. (a) Internal drop temperature versus radius with diffusion regime boundary condition and 0 °C initial temperature: after 10 μs (solid curve), 20 μs (dotted curve), 30 μs (dashed curve). (b) Internal drop temperature versus radius with fixed temperature (100 °C) boundary condition and 100 °C initial temperature: after 10 μs (solid curve), 20 μs (dotted curve), and 30 μs (dashed curve). (c) Central drop temperature versus time for the case given in part (b).

perature after the fast heating phase corresponds to a steady-state parabolic internal temperature profile that evolves parametrically as the drop radius shrinks in time.

To understand better why the drop radius never changes substantially before the interior heats to a maximum temperature, for any given laser flux, consider the ratio of $\tau_{\rm evap} \equiv (1/r_d)(dr_d/dt)^{-1}$ to $\tau_{\rm temp} \equiv (1/T) \times (\partial T/\partial T)^{-1}$ defined at the drop center. If we consider Eqs. (1) and (2) and neglect the thermal diffusion term in Eq. (2) we arrive at the estimate

$$\frac{\tau_{\rm evap}}{\tau_{\rm Temp}} \approx \frac{(\frac{4\pi}{3} r_d^3 \rho_l) L}{[4\pi r_d^2 \kappa_w (\partial T/\partial r)|_{r_d -}] c_w T/3} \equiv \left| \frac{dQ_{\rm abs}}{dQ_{\rm surf}} \right| \frac{3L}{C_w T} \approx 5 \left| \frac{dQ_{\rm abs}}{dQ_{\rm surf}} \right| , \tag{17}$$

where $dQ_{\rm abs}$ and $dQ_{\rm surf}$ are the rate of energy absorbed volumetrically and given off at the drop surface, respectively. We define being in the heating phase by $|dQ_{\rm abs}/dQ_{\rm surf}| \gg 1$, that is, the rate of energy absorption by the drop is much greater then the rate at which energy is lost at the drop surface. With this Eq. (17) says that $\tau_{\rm evap} \gg \tau_{\rm Temp}$ and thus the drop center temperature rises fast compared to the change in radius. However, for this to be valid we had to neglect the thermal diffusion term in Eq. (2). Again, from Eq. (2) we can estimate the ratio of the thermal diffusion time $\tau_{ThD} \equiv r_d^2 \rho_w c_w / \kappa_w$ to $\tau_{\rm Temp}$ as

$$\frac{\tau_{ThD}}{\tau_{\rm Temp}} \approx \frac{[(4\pi/3) r_d^3 \rho_l]}{(1/3)[4\pi \kappa_w r_d^2 (T/r_d)]} \approx 3 \left| \frac{dQ_{\rm abs}}{dQ_{\rm cond}} \right| , \tag{18}$$

where $dQ_{\rm cond}$ is conductive heat flux. However, as readily seen from a comparison of Eqs. (17) and (18) $dQ_{\rm cond} \approx dQ_{\rm surf}$ for a temperature gradient scale length of drop dimensions. Thus $\tau_{ThD} \gg \tau_{\rm Temp}$, again by virtue of the fact that one is in the heating phase.

In Fig. 2 is shown a water drop phenomenology map for 10.6-μm laser irradiation that summarizes the numerical results of our model for a given initial drop size and laser flux (unlimited fluence is assumed). Results for drops with radii between 0.5 and 20.0 μm are shown. The bound-

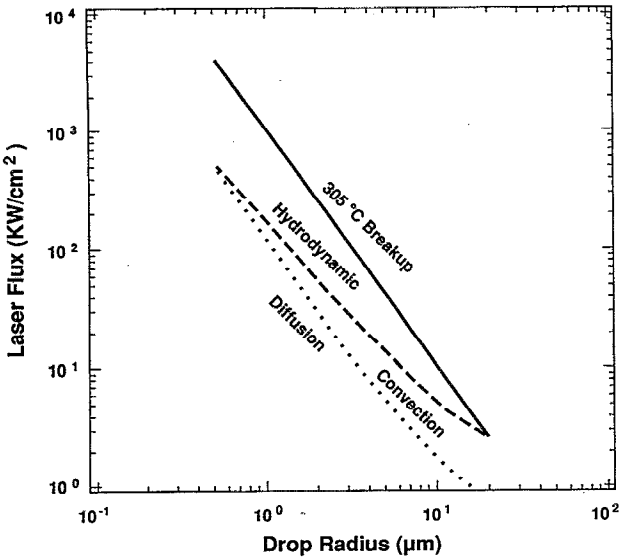

FIG. 2. Phenomenology diagram: Diffusion regime is below dotted curve; convection regime is between dotted and dashed curves; hydrodynamic regime is above dashed curve; 305 °C breakup regime is above solid curve.

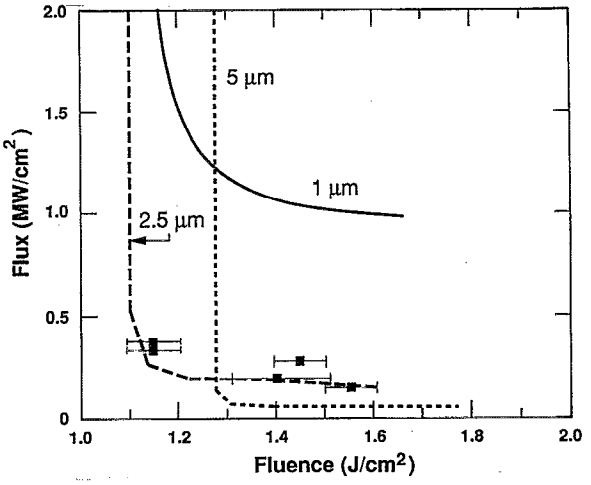

FIG. 3. Theoretical flux versus fluence curves to achieve internal explosion for three drops with the indicated initial radii. Solid squares with error bars are experimental data.

ary of the diffusion and convection regimes is given by the dotted curve, defined by $A=1$. The diffusion regime lies in the lower left-hand corner which consists of sufficiently small drop size and laser flux. The convection regime is bounded by the dotted and dashed curves. The dashed curve is the boundary where the drop surface temperature reaches boiling at one atmosphere pressure and thus where the steady-state two fluid flow boundary condition on T_s, given by Eqs. (16) and (8), breaks down. The solid curve is the boundary where a 305 °C superheat temperature is achieved in the drop center. This is found to be well described by the expression

$$\text{Flux}(\text{kW/cm}^2) \approx 50[25/r_d^2(\mu\text{m})], \tag{19}$$

and appears to be in agreement with previous studies.[7,8] (Note in particular the result given in Ref. 8 of 13 kW/cm^2 as the threshold of explosive boiling for a 10-μm radius drop.) The region between the dashed and solid curves is the stable superheating regime. In this regime complicated hydrodynamic flow (shock waves, for example) may occur outside the drop. Above the solid curve a drop explodes from the center. Because we assume volume absorption the curves are not continued for drops with radii greater than 20.0 μm. For drops less than 0.5 μm the given curves may simply be continued as straight lines.

Figure 3 gives the laser flux versus fluence to achieve the unstable 305 °C central temperature for the three indicated initial drop radii. The small differences in these curves at the high laser flux part of the figure (2 MW/cm^2) is due to small differences in the absorption coefficients. As the flux threshold to attain this central temperature is reached more fluence is needed. Finally, the drop radius decreases enough during the heating process that for a given flux level 305 °C is not attained in the center. For this reason the curves in Fig. 3 terminate with a small but finite slope and are not asymptotic to any horizontal line.

III. MULTIPLE DROP CLOUD MODEL

Our multiple drop cloud model consists first of an equation for the laser intensity $I(z,t)$ as a function of the spatial coordinate along the beam, z, and the time, t

$$\frac{dI}{dz} = -\gamma(z,t)I, \tag{20}$$

where γ is the total attenuation due to both Mie scattering and absorption by water drops,[1,2] as well as from direct air absorption. By writing the propagation equation for a beam in this one-dimensional form, without consideration of multiple scatterings, it is implicitly assumed that the beam diameter is sufficiently small that light scattered out of the beam does not scatter again in the beam channel and is thus lost from the calculation. This is a good approximation for most actual cloud conditions and for beam diameters less than a few meters and gives a lower bound on clearing beam efficiency. For our experiment this assumption simply means that scattered light is not received by the far-field detectors.

The distribution of drops at any time, t, and at any point along the beam, z, is divided into groups of $N_{i,j}(z,t)$ drops per cm^3, where the index i corresponds to the initial drop size of a group, and j corresponds to the mass of nonwater solute in a drop. This discretization is used to obtain a deterministic set of ordinary differential equations that describe drop evolution such that no two evolutionary curves in the (z,i,j) phase space with different initial conditions can cross.

A. Low laser flux and natural recondensation model

If we consider the cloud drops to have a uniform temperature $T_{i,j}(z,t)$ in their interiors that simply varies with

time, and a total water mass $m_{i,j}(z,t)$, we can construct a model appropriate to low laser flux and natural recondensation as follows. First, multiply Eq. (2) by r^2 and integrate over the drop volume using Eq. (1) at the drop surface. This gives for the time evolution of the drop temperature the result

$$m_{i,j}c_w\frac{dT_{i,j}}{dt}=P_{i,j}+L\frac{dm_{i,j}}{dt}-4\pi\kappa_a r_{i,j}(T_{i,j}-T_a), \quad (21)$$

which expresses energy conservation. To obtain an equation for the evaporation (recondensation) rate in the diffusion regime we use mass conservation $(dm_{ij}/dt) = -4\pi r_d^2\Gamma$ in conjunction with the simplified form of Γ given by Eq. (10). This results in

$$\frac{dm_{i,j}}{dt}=4\pi D r_{i,j}(\rho_{v\infty}-\rho_{wv(i,j)}), \quad (22)$$

where $\rho_{wv(i,j)}$ is the water vapor mass density over the surface of a drop of group i,j at temperature $T_{i,j}$ and is a generalization of the quantity $\rho_s(T_s)$ in Eq. (10). (This can be found in many books;[9-12] we follow the treatment given in Ref. 9.) This is given by

$$\rho_{wv(i,j)}=\rho_{\rm sat}(T_a)\left(1+\frac{LM_w}{RT_a^2}(T_{i,j}-T_a)\right)\times\left[\left(1+\frac{a_{i,j}}{r_{i,j}}\right)\Big/\left(1+\frac{b_j r_{s,j}^3}{(r_{i,j}^3-r_{s,j}^3)}\right)\right]. \quad (23)$$

The first term in brackets is a lowest order linearization of the Clausius–Clapeyron equation at the drop temperature $T_{i,j}$ and about the ambient air temperature T_a. The quantity $\rho_{\rm sat}(T_a)$ is the saturated water vapor mass density at T_a, and from Eqs. (4) and (5) is given by

$$\rho_{\rm sat}(T_a)=\left(\frac{M_w}{RT_a}\right)p_r e^{(LM_w/R)(1/T_r-1/T_a)}. \quad (24)$$

The quantities $a_{i,j}$ and b_j in the second bracket of Eq. (23) modify $\rho_{wv(i,j)}$, due to surface tension and solute concentration, respectively. The water vapor density over a solid core is zero as given by Eq. (23), as it must be. In terms of the above quantities the water mass content $m_{i,j}$ of the drop is given by

$$m_{i,j}=\tfrac{4\pi}{3}\rho_w(r_{i,j}^3-r_{s,j}^3), \quad (25)$$

where $r_{i,j}$ is the radius of drops of the group (i,j), $r_{s,j}$ is the radius of the dry solute or nucleation core, and the mass difference between water and the dry core has been neglected.

The average water vapor mass density, $\rho_{v\infty}$, is determined by water mass conservation. It is usually initialized at $\rho_{\rm sat}(T_a)$ using Eq. (24) and evolves in time due to drop vaporization, recondensation, and changes in the air temperature. The air temperature, T_a, is determined by energy conservation. It evolves in time due to thermal conduction from the heated water drops, temperature equilibration of the evaporated water vapor with the air, and direct heating of the air via laser absorption. The model as solved numerically is stated in the Appendix.

B. Physical interpretation

With regard to the form and the range of validity of the model given by Eqs. (20)–(25) the following points are stressed. First, it is necessary for the distribution of drop sizes with time to be a function of both initial drop size distribution and solute mass. This two-dimensional form is needed because in the course of evaporation and recondensation the rates of these processes for a drop of a given size are different for different dissolved nonwater content. It is possible, for example, for two drops with different initial sizes to exchange order of sizes during recondensation. Because drops with more solute recondense faster, an initially smaller drop with more solute can overtake and pass in size a drop that was initially larger but had less solute. Even a water drop initially larger than another one of the same type (same total nonwater content) may under laser irradiation become the same size because it is for a time more effective in absorbing laser energy. Even so, these two drops may then not necessarily be considered identical since they may still have different temperatures. If the laser is turned off, then they will become identical because of thermal conduction to the air after a period of time. Only if both drops are reduced to their dry aerosol cores can they with certainty be considered identical. As the drop radius decreases the thermal conduction to the air will eventually balance the laser power absorbed (proportional to the water volume for small drops) achieving a steady state unless the dry aerosol cores themselves are significantly absorbing. It is thus computationally convenient not to ever merge the different number densities, $N_{i,j}$, initially associated with a given drop type j. As previously mentioned, the two terms in the first set of brackets on the right-hand side of Eq. (23) result from the linearization of an exponential. For this to be a good approximation the increase in $T_{i,j}$ over T_a must be no more than about 15 °C, which is generally not satisfied when drops are heated to their boiling point. However, this does not matter during the vaporization phase since the rate of vaporization is not determined by the water vapor density just outside the drop, but by the absorbed laser energy that goes into vaporization. That is, since the model conserves total energy and total water mass the correct vaporization rate is automatically achieved. The important regime for the linearization is in the recondensation phase where $P_{i,j}=0$. The drop temperature equilibrates rapidly to the air temperature so that the quoted restriction is well satisfied. Finally, the model assumes that recondensation does not take place until the water vapor from the evaporating drops has had time to become uniformly distributed in space. This assumption is addressed after the high laser flux model is discussed.

The physical content of the model just given can most easily be explained with the help of the curves shown in Fig. 4. These curves are known as Kohler curves and are derived from considering a drop to be in equilibrium with its surrounding vapor. From Eq. (22) this requirement is that $\rho_{wv(i,j)}=\rho_{v\infty}$. Suppressing the (i,j) subscripts, restoring the exponential in Eq. (22), and relabeling the drop surface temperature $T_{i,j}$ as T_d we have

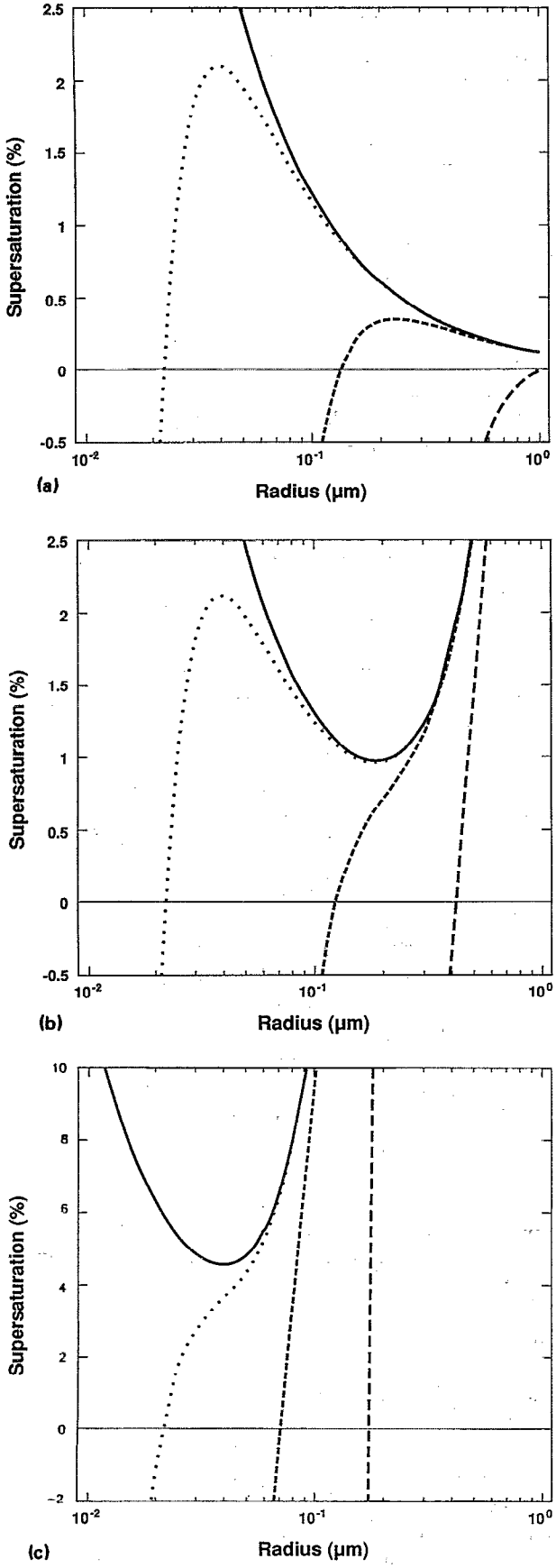

FIG. 4. Kohler curves. (a) For zero laser flux: surface tension barrier (solid curve); for drops with dry salt cores of radii 0.0075 μm (dotted curve), 0.025 μm (dashed curve), and 0.10 μm (dash-dot curve). (b) For a laser flux of 100 W/cm^2. (c) For a laser flux of 10 kW/cm^2.

$$\%S_{\text{sat}} = 100\left(\frac{(1+a)/r}{[1+br_s^3/(r^3-r_s^3)]} \times \exp\frac{LM_w}{R}\left(\frac{1}{T_a}-\frac{1}{T_d}\right) - 1.0\right)$$

$$\approx 100\left(\frac{a}{r} - \frac{br_s^3}{r^3} + \frac{LM_w p_l r^2}{RT_a^2 3\kappa_a}\right), \tag{26}$$

where $\%S_{\text{sat}} = 100[\rho_{v\infty} - \rho_{\text{sat}}(T_a)]/\rho_{\text{sat}}(T_a)$ is the supersaturation of the air in%. Since a water drop can be in equilibrium in the presence of an irradiating laser beam, the drop and background air temperatures may be different. (This is the major change here from the usual treatment.) From the steady-state limit of Eq. (21) the drop surface temperature is

$$T_d = T_a + \frac{p_l r^2}{3\kappa_a}. \tag{27}$$

This expression is used in Eq. (26) in both the exponential factor and in the surface tension coefficient a. In order that Eqs. (26) and (27) be valid T_d must be less than boiling. Thus for $T_d - T_a = 100\,^\circ$C, Eq. (27) requires that $r_d \leqslant 84\ \mu\text{m}/[I^{1/2}(\text{W/cm}^2)]$ for this to be true. Note from the approximate form of Eq. (26) that it consists of essentially three terms, the surface tension term $\sim 1/r$, the solute term $\sim -1/r^3$, and a laser flux term $\sim r^2$. It is the interplay of these three terms that form the basis for the physical interpretation of natural cloud formation, slow, nonexplosive evaporation, and recondensation.

Let us now consider what happens to water drops in equilibrium with their background as a function of laser flux. First we treat the case of zero laser flux ($p_l = 0$) that is also the situation relevant to natural cloud formation. This is shown in Fig. 4(a). The solid curve is the case where the water drop has a solid, insoluble nucleation core. That is, $b=0$, and only the surface tension term contributes in Eq. (26). Only one equilibrium point is possible and for this to occur the supersaturation level must be greater than zero. From Fig. 4(a), given a 2% supersaturation level a wetted solid core must be greater than 0.06 μm in radius in order to grow as a large cloud water drop. Solid, insoluble aerosols smaller than this will not wet at this supersaturation level. They reside inside the surface tension "barrier". This is the same barrier that prevents homogeneous nucleation unless large supersaturations are present. This is because nucleation cores that are due to statistical fluctuations are considerably smaller than atmospheric aerosols. Next the dotted, dashed, and dash-dot curves in Fig. 4(b) are for drops with pure salt nucleation cores ($b=1.37$) with dry radii of 0.0075, 0.025, and 0.10 μm, respectively. Because of this the term $\sim 1/r^3$ in Eq. (26) dominates at small radius and an additional equilibrium point is introduced. This equilibrium point resides on a curve with positive slope and is stable to perturbations in the supersaturation level, while the equilibrium point where the curve has negative slope is unstable. To see this consider the dotted curve and a supersaturation level of 1%. There are equilibrium points at radii of about 0.021

μm (positive slope) and 0.10 μm (negative slope). If the supersaturation level is increased the 0.021-μm radius equilibrium point will shift slightly upward along the dotted curve increasing slightly in size. However, the 0.10-μm radius equilibrium point would also have to rise vertically resulting in a decrease in size to find its correspondingly new equilibrium point. But this is not energetically favorable because the supersaturation level has increased and from Eq. (22) dm/dt must be positive. Thus this drop grows to the right limited only by a decrease in the supersaturation level due to recondensation. That is, the only way it can find a new equilibrium point is by a change in the background water vapor level—a nonlinear effect. By an analogous argument if the supersaturation level is perturbed downward the 0.021-μm radius drop shifts down slightly but the larger 0.10-μm drop cannot find a new equilibrium point unless it evaporates all the way to the smaller, stable equilibrium point. For the stable 0.021-μm radius drop to become a large cloud drop the supersaturation level must increase above 2% for it to cross over to the unstable part of the Kohler curve. For negative supersaturations only the stable equilibrium point exists.

In the formation of clouds only the largest and most soluble aerosols become cloud drops. However, there is believed to be a large number of core aerosols present that are wetted and sit at the stable equilibrium point but have much smaller condensed water content.[13] These smaller wetted aerosols at their stable equilibrium points are called "inactive". The larger droplets to the right of the unstable point are said to be "active". The inactive aerosols may be able to climb over the peak of their Kohler curves if there is a sudden increase in the level of supersaturation. Likewise, active cloud drops that are evaporated to a small size may not be able to reform if the supersaturation level after laser irradiation is insufficient. All this depends on the time history of the level of supersaturation. This highlights the fact that recondensation after laser irradiation can be rather complicated.

Next consider in Fig. 4(b) what happens to the equilibrium curves of Fig. 4(a) if we include a constant 100 W/cm^2 CO_2 laser beam incident on the respective drops in a background air temperature $T_a = 0$ °C. Because the added laser flux term in Eq. (26) is positive and parabolic, the unstable part of the Kohler curves in Fig. 4(a) will for large enough radii turn positive in slope and become stable, as shown in Fig. 4(b). (Note the minimum in the surface tension barrier curve.) From one to three equilibrium points may occur and correspondingly complex drop evolutions may result. If a supersaturation level above the minimum in the surface tension curve is achieved (greater than about 1% in this case) then all initial cloud drops regardless of their nucleation core constitutency will reform after the laser is turned off, since then the Kohler curves revert to those shown in Fig. 4(a) and all of these drops will be out of equilibrium and above the surface tension curve and will thus grow limited only by the water vapor available. In addition, inactive drops that are able to rise over the peak of their natural Kohler curves while the laser is on due to enhanced supersaturation levels will also grow when the laser is turned off. Thus the result will be that there are at least as many if not more drops than initially present before the laser was turned on. In order for recondensation to be inhibited supersaturation levels must be low enough and drops evaporated small enough that when the laser is turned off they reside on the stable portion of their respective Kohler curves. In a laboratory cloud composed of drops of pure water (no nucleation cores) all drops will be evaporated to the same size for a long enough laser pulse. Then if the supersaturation level is raised above the minimum of the surface tension curve, when the laser is turned off all drops will grow, otherwise all drops will have evaporated. Thus, unless there are substantial nucleation sites due to aerosols, one should see a sharp boundary in recondensation level that is an equally sharp function of initial cloud water content.

In Fig. 4(c) is shown curves corresponding to those in Fig. 4(b) except that the laser power has been increased to 10 kW/cm^2. Note that the minimum in the surface tension curve has been displaced vertically by more than a factor of four and shifted in radius from about 0.11 to about 0.04 μm.

Next we consider the relative importance of water vapor and thermal diffusion to the recondensation process. It is readily seen from Eqs. (21)–(23) that if either D or κ_a, the diffusivity or thermal conductivity of air, is zero then no recondensation can take place. The relative importance of these two processes [c.f., Eq. (A5) of the Appendix] can be ascertained from the size of the dimensionless parameter Λ defined as

$$\Lambda \equiv \frac{\kappa_a R T_a^2}{M_w D \rho_{\text{sat}} L^2} \propto \frac{T_a p_{\text{air}}}{\rho_{\text{sat}}}, \tag{28}$$

where p_{air} is the air pressure. Because of the strong increasing dependence [the Clausius–Clapeyron equation, c.f., Eq. (24)] of ρ_{sat} on T_a, Λ is a decreasing function of T_a. Thus if $\Lambda \gg 1$, $dm/dt \sim D\rho_{\text{sat}} r \times$ (supersaturation) so that recondensation is water vapor diffusion limited. If $\Lambda \ll 1$, $dm/dt \sim \kappa_a T_a^2 r \times$ (supersaturation) and recondensation is thermal conduction limited. For an air pressure of 0.75 atm we find that $\Lambda = 0.32$ at 20 °C and 4.77 at -20 °C. The crossover point ($\Lambda = 1$) is at about 0 °C, depending somewhat on p_{air}. In particular, for a given constant value of supersaturation and decreasing air temperature we expect the rate of recondensation to be much slower for $\Lambda \gg 1$ than for $\Lambda \ll 1$, owing to the exponential dependence in Eq. (24).

C. High laser flux model

As already mentioned, cloud water drops irradiated with high enough laser intensity may superheat and possibly explode. We now show how we can accommodate both of these phenomena in a full cloud model in an approximate manner.

First, from combining Eqs. (21)–(23) an equation that gives the water drop temperature in the low laser flux regime can be derived [this is given as Eq. (A4) in the Appendix]. This equation is used to indicate when a drop

has been heated to its boiling point. (At this point, from single drop studies, drops do not show a significant temperature gradient.) If this occurs we solve an approximate form of Eqs. (1) and (2) for the internal drop temperature of that (i,j) group with the initial drop temperature uniform at the boiling point and with the simple boundary condition $T_s(r_d,t) = T_b$ fixed in time. To construct an approximate form of Eqs. (1) and (2) we utilize an assumed functional form for $T(x,t)$ interior to the drop, choosen as $T(x,t) = T_0(t) - [T_0(t) - T_b]x^{n(t)}$. From this a very accurate approximation to Eqs. (1) and (2) is constructed consisting of three ordinary differential equations (ODEs) for $r_d(t)$, $T_0(t)$, and $n(t)$. A detailed discussion of this representation and its accuracy is given in Ref. 14. These three equations form the high laser flux heating model. If the temperature T_0 at the drop center reaches or exceeds 305 °C the drops are exploded. Since we do not know the precise dynamics of this, we construct a simple phenomenological description. We quantify drop explosion by two parameters. The first, the drop splitting factor, gives the number of drops into which a single drop divides when it explodes. Thus $N_{i,j}(z,t)$ is increased by this factor when drops of the group (i,j) at the location z explode. The second parameter gives the fraction of the superheat energy stored in the drop that goes into direct conversion of liquid water into vapor during the explosion. The internal drop temperature after the explosion is set to be either flat at T_b, or to a parabolic function with value T_b at the edge, depending on how much of the superheat energy is retained. Mass and energy are both conserved in this process. This simple model allows for multiple explosions of a single initial drop since if for a given laser flux one explosion event results in water fragments that are not small enough to be below the explosion boundary given in Fig. 2, the fragments will simply heat more until they explode again. This property makes the end result somewhat insensitive to the precise value of the drop splitting factor. All during the superheat phase of any drop group the drop temperature equation used in the low flux model, Eq. (A4), is solved. If that equation indicates a drop group temperature below the boiling point, which will always happen if the drop size becomes small enough, the equations are switched to the low laser flux model.

Drop explosion can make the vaporization of cloud drops more efficient since when the drops become small due to breakup, with say the same water mass, they still absorb the same laser energy since absorption depends only on water volume, but they scatter light out of the beam less efficiently. This is particularly true if the drop fragments become small enough to be in the Rayleigh regime for the particular laser wavelength in question. For 10.6-μm laser light and drops in the 5-μm radius size range we find that initially about 60% of the incident light is scattered at least once and 40% is absorbed in an optically thick cloud.

Recondensation occurs only using the low laser flux model equations wherein the energy and water vapor associated with drop vaporization is deposited uniformly with respect to the background air. We assume that recondensation occurs on the residual of the original drop, which may be increased in number due to drop explosion, or on haze nuclei (small drops at the Kohler stable point). Thus drop explosion may result in a much increased recondensation rate, after the laser is turned off and the water vapor has diffused to an approximately uniform state, since each original drop may result in many smaller drops, each serving as a recondensation site. The model does not treat large transient gradients in temperature and water vapor outside a water drop during or just after vaporization. Since the diffusion coefficient for heat is somewhat smaller than the diffusion coefficient for water vapor in air, the water vapor spreads out somewhat faster from a vaporized drop than the heat.[15] Thus large supersaturations (from the Clausius–Clapeyron equation) much above that which would occur from just a uniform deposition of water vapor leading to very rapid recondensation in the plume even without nucleation cores (homogeneous nucleation) are not expected to occur. In any case, we must consider the timescales for significant recondensation arrived at from this model to be upper bounds on actual recondensation times.

For an optically thick cloud a bleaching front will occur at the head of the laser pulse where water drops are just being evaporated.[16] From the relevant parameters of the model we can construct the velocity characteristic of the laser penetration process as $I_0/\rho_c\tilde{L}$, where I_0 is the unattenuated laser intensity, ρ_c is the condensed water content, and $\tilde{L}$ is the latent heat of vaporization at the boiling point modified to include the energy deposited into the drop to raise its temperature from that of the surrounding air to boiling. So, defining γ_{eff} as the fraction of the laser intensity that is absorbed we have

$$v_{\text{bleach}} \approx \frac{\gamma_{\text{eff}} I_0}{\rho_c \tilde{L}} . \tag{29}$$

For $\gamma_{\text{eff}} \approx 0.57$, appropriate for the 10.6-μm wavelength, and $I_0 = 1$ MW/cm^2, $\rho_c = 0.05$ g/m^3 we have $v_{\text{bleach}} = 40.0$ m/μs, typically.

IV. SIMULATION RESULTS

Utilizing the multiple drop cloud simulation code we present comparisons with experimental data obtained from the Meteor 2 laser. Meteor 2 is an *e*-beam initiated *DF* $\rightarrow$ CO_2 chemical transfer laser. Single pulse energies up to 360 J, with typical pulse lengths of 25 μs are common. In Fig. 5(a) is shown the output pulse of this laser which we use in the forthcoming calculations. This pulse is uniform over a 5-cm-diam channel and fired through an 80-cm-long cloud chamber.[17] The laser pulse in Fig. 5(a) contains 9.7 J/cm^2 of fluence. The cloud chamber has a condensed water content of 2.2 g/m^3 and is at 0% supersaturation at 27 °C. The measured water droplet distribution is peaked at 2.5 μm in radius and is given in Table I. This distribution is found to be nearly independent of the total condensed water content of the cloud chamber. Although this size distribution is not typical of most natural clouds, it is quite satisfactory for the studies undertaken here.

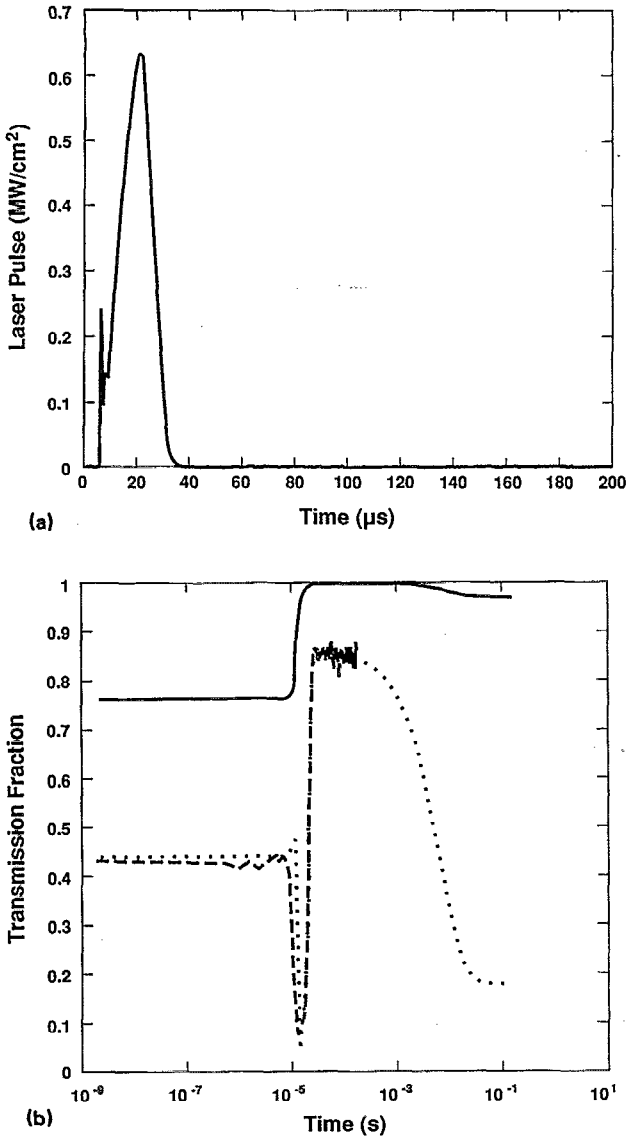

FIG. 5. (a) Meteor 2 laser pulse vs time. (b) Transmission fraction vs time: experimental data 5145 Å probe beam (dashed curve), simulation probe beam (dotted curve), 10.6 μm clearing beam (solid curve).

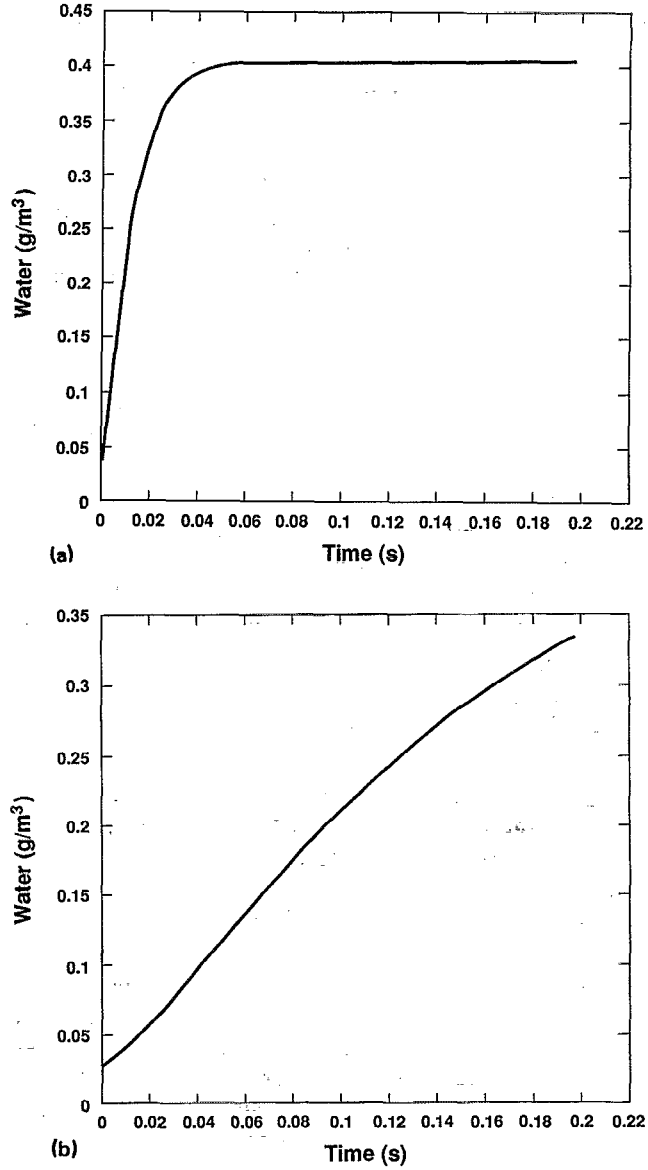

FIG. 6. Recondensation rate vs time after laser is turned off. (a) Droplet shattering. (b) No droplet shattering.

In Fig. 5(b) is shown the transmission fraction through the cloud chamber. The dashed curve is experimental data for the first 100 μs obtained from a 5145Å probe laser. The dotted curve is the simulation result at that wavelength. The solid curve shows the simulated transmission of the 10.6-μm clearing beam. The simulation is run for 0.2 s and shows both the sharp decrease in transmission of the probe laser due to droplet shattering at about 10 μs and the gradual decrease in transmission due to recondensation after the laser is turned off. Agreement with experiment for the first 100 μs is excellent. Note that there is no drop in transmission of the clearing beam when the drops shatter. This is because the water drops are volume absorbers so that the distribution of total water content does not effect absorption. Also, when drops that are already smaller than a given wavelength divide they scatter less effectively to that wavelength, a point we shall return to shortly. The experimentally measured time to shatter for a given laser pulse shape allows the flux versus fluence to shatter to be plotted against the theoretical predictions. This is indicated for the 2.5-μm radius drop results shown in Fig. 3. The square boxes with indicated error bars give the experimental result. The agreement is excellent. In Fig. 6 we show the effect that droplet shattering can have on the rate of recondensation. Here is shown the condensed water content versus time after laser termination, part (a) is with droplet shattering and part (b) is without. Note that the maximum amount of recondensed water expected from the

TABLE I. Drop distribution.

Size (μm)	1	1.5	2	2.5	3	4	5	6
# (%)	10.6	14.1	17.7	19.4	17.7	14.1	5.7	0.7

Clausius–Claperyon equation is reached about a hundred times more quickly when the droplet shattering model is used because of the large number of additional recondensation sites.

Next we consider how a 10.6-μm CO_2 laser can be used to clear a channel with respect to the 3.8-μm wavelength with a minimum of fluence utilizing a flux high enough to shatter drops but only partially vaporize them. If drops breakup sufficiently then scattering at the 3.8 μm can be dramatically reduced if the Rayleigh regime is reached. Because the CO_2 clearing beam is still absorbed volumetrically by the remaining liquid water we can only hope to clear, at the 3.8-μm wavelength using a low fluence, thin clouds in which the 10.6-μm wavelength is not initially attenuated more than about one *e*-folding.

Consider how the relative scattering of a water drop changes due to it dividing into N drops and, for simplicity, with no evaporation (some substantial evaporation will occur since the stored superheat energy is considerable). If R is the ratio of scattering after droplet division to that before, we have

$$R=\frac{NQ_a\pi r_a^2}{Q_b\pi r_b^2}=\frac{Q_aN^{1/3}}{Q_b}=\frac{Q_a}{Q_b}\frac{r_b}{r_a}, \tag{30}$$

where Q is the dimensionless scattering crossection and r is the droplet radius; the subscripts b and a indicate before and after scattering, respectively.

As can be seen from Eq. (30), if $Q_a \approx Q_b$ then scattering increases after shattering. This is seen as a sharp decrease in transmission as given in Fig. 7(a) for the 1.06-μm probe. In general, Q peaks at a value of about 3.8 for $r_d/\lambda = 1$, where r_d is drop radius and λ is the wavelength of the light being scattered. The Rayleigh regime begins at $r_d/\lambda \leqslant 0.3$ where $Q \approx 0.5$.[18] Thus for $\lambda = 3.8$ μm, $r_d \leqslant 1.14$ μm is the Rayleigh regime where $Q \sim r_d^4$. So, from Eq. (30), changing the drop radius a factor of two ($N=8$) by scattering would reduce net light scattering by a factor of 8 in the Rayleigh regime.

In Fig. 7(a) we show transmission as a function of time for a 10.6-μm clearing beam and for 1.06-μm and 3.8-μm passive probe beams through a cloud 0.5-kM thick with a liquid water concentration of 0.01 g/m^3. For clarity of interpretation we choose all drops to be 5 μm in radius (19 drops/cm^3). In Fig. 7 the 10.6-μm laser pulse has a flux of 0.5 MW/cm^2 and a 10 μs duration so that the total fluence is 5 J/cm^2. Figure 7(a) shows transmission through the cloud as a function of time. Note the sharp decrease in transmission of the 1.06-μm probe (dashed curve) in Fig. 7(a) corresponding to drop shattering. The 3.8-μm probe (dotted curve) does not show this decrease in transmission because of its smaller initial ratio of r_d/λ and consequently clears to a 98% level after 10 μs. The solid curve is the 10.6-μm clearing pulse. The 1.06-μm probe remains opaque due to the fact that the drops do not become small enough to reach the Rayleigh regime with respect to this wavelength. Figures 7(b) and 7(c) give the drop size and number, respectively, as a function of distance through the cloud at 20 μs (10 μs after the laser has turned off). The drops explode either four or three times

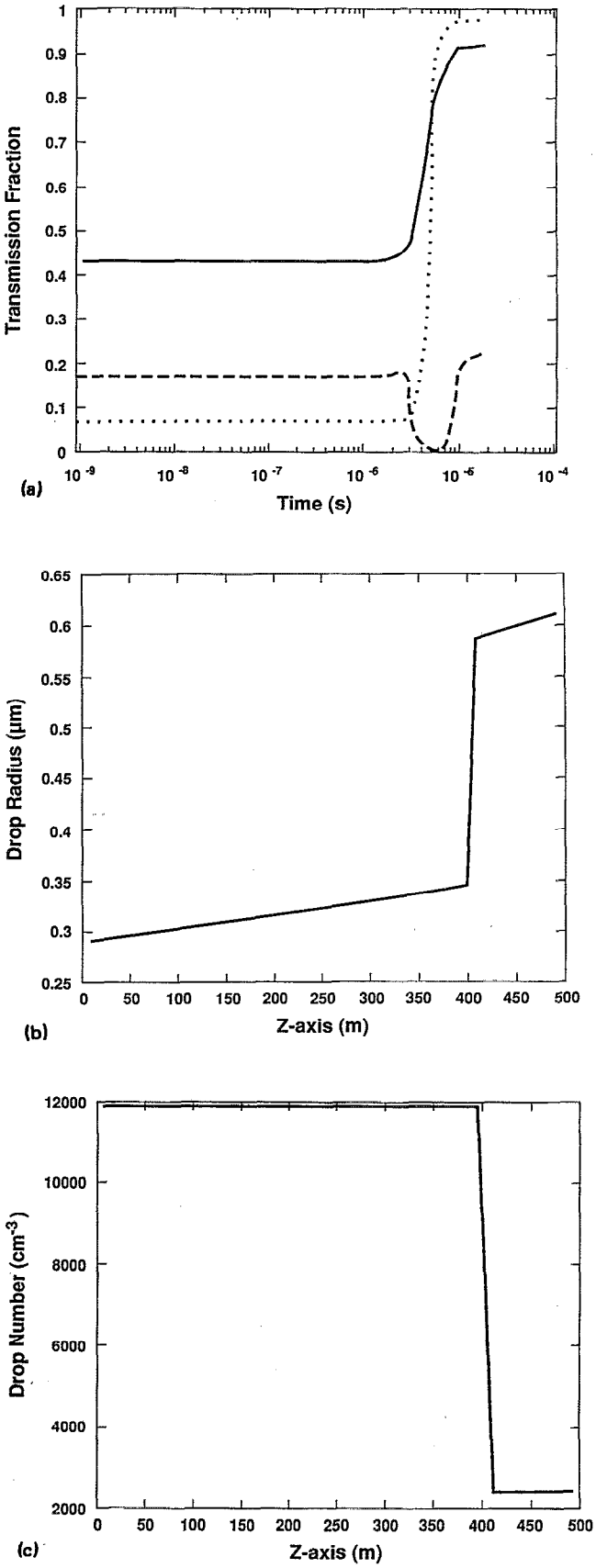

FIG. 7. (a) Transmission fraction vs time for a 0.5 MW/cm^2, 5-J laser pulse: 10.6 μm clearing beam (solid curve); 3.8-μm probe beam (dotted curve); 1.06-μm probe beam (dashed curve). (b) Drop size vs distance 10 μs after laser termination. (c) Drop number vs distance 10 μs after laser termination.

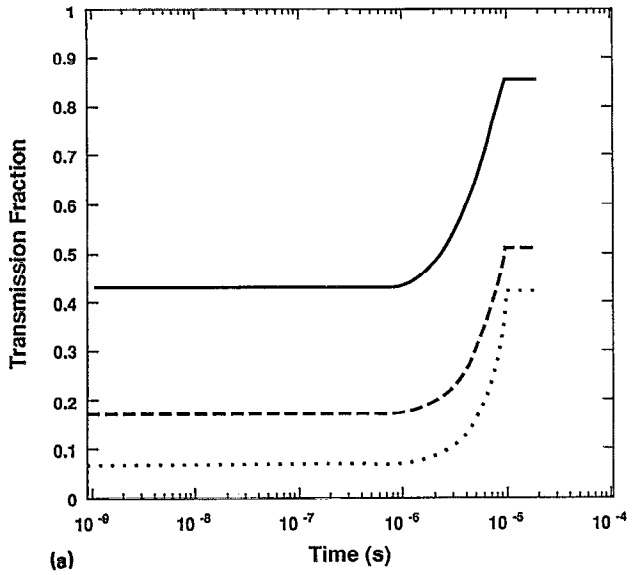

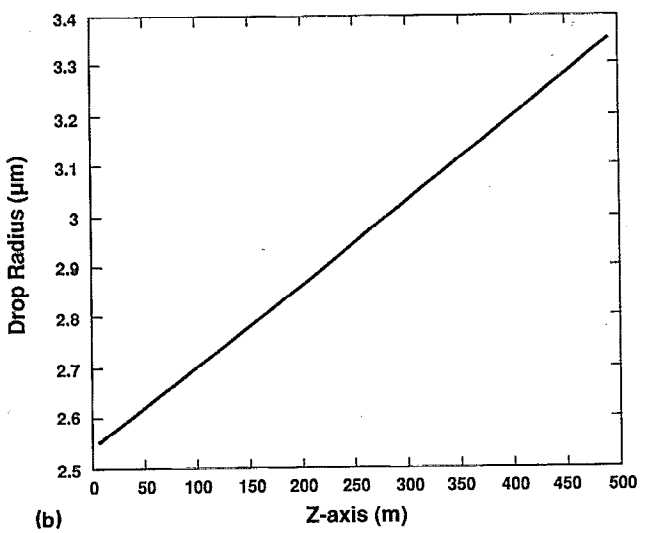

FIG. 8. (a) Transmission fraction vs time for a 0.5 MW/cm^2, 5-J laser pulse but without drop shattering: 10.6-μm clearing beam (solid curve); 3.8-μm probe beam (dotted curve); 1.06-μm probe beam (dashed curve). (b) Drop size vs distance 10 μs after laser termination.

[note the sharp jump in Figs. 7(b) and 7(c)] into five pieces per generation resulting in drops with about a 0.35-μm radius. (Evaporation is also included.) These results are not overly sensitive to how many pieces a drop breaks into on a single shattering event since shattering will continue to occur until drops smaller than the shattering barrier of Fig. 2, for the given flux, are obtained.

In Fig. 8 we show the same case except that now no drop shattering, only evaporation, is included. Fig. 8(a) shows the transmission versus time for the same laser beams as given in Fig. 7(a). Note that the probe beams do not show a great degree of increased transmission and that the 3.8-μm probe does not come up to 50% transmission. The reason for this is readily seen in Fig. 8(b) where the mean drop size versus distance through the cloud is given and is seen to be about 3 μm in radius. This means about 80% of the liquid was converted to vapor, but not much clearing occurred. The droplet density was the same as the initial value previously given.

In Fig. 9(a) we show transmission results with droplet shattering for the same parameters as in Fig. 3(a) but for a pulse time of 6 μs (3 J/cm^2). This shows the effect of lower fluence for other parameters held constant. Even with 3 J/cm^2 we see that there is 90% transmission for the 3.8-μm probe after 6 μs of laser irradiation. Note that for this case the 1.06-μm probe transmission decreases due to droplet shattering but does not recover due to a smaller amount of liquid water evaporation than in the case shown in Fig. 7(a). Finally, in Figs. 9(b) and 9(c) we show transmission as a function of time for the same parameters as in Fig. 7(a) except that we lower the laser flux and extend the pulse time so that the total fluence remains the same at 5 J/cm^2. In Fig. 9(b) the results shown are for a 10.6-μm clearing laser with a flux of 0.25 MW/cm^2 and pulse length of 20 μs. In Fig. 9(c) the laser flux is 0.1 MW/cm^2 and the pulse length is 50 μs. For the 0.25 MW/cm^2 case 5 J/cm^2 of fluence is still effective in clearing the 3.8-μm probe to over 90% while for the 0.1 MW/cm^2 case this is not the result and the cloud remains opaque.

Thus, we have shown that for improved transmission at 3.8 μm only a modest investment in 10.6-μm laser fluence is required if the laser flux is high enough to induce sufficient droplet shattering. This is at least an order of magnitude lower in fluence than would be required to clear a comparable cloud for wavelengths on the order of or less than 1 μ.

Finally, we consider the scenario proposed previously[19] wherein an ice cloud can be cleared simply by melting the ice crystals and allowing them to freely evaporate. This scenario is somewhat simplistic and we only consider it briefly.

Because the the Clausius–Clapeyron Eq. (24) is a strongly increasing function of the temperature T_a small changes in air temperature (a few tenths of a degree K are very significant in lowering the supersaturation level and inhibiting recondensation. Also, the amount of water vapor retained in the air is a strong function of T_a. For ice clouds the implications of Eq. (24) are very important because L, the energy to go to the gaseous phase, acquires in addition to the latent heat of vaporization (about 540 cal/g) the latent heat of fusion, an extra 80 cal/g. Because of this a cirrus ice cloud at 0% supersaturation with respect to ice is undersaturated with respect to supercooled water at the same temperature. If there is no refreezing or direct recondensation to ice, then a quantity of ice turned to water vapor can be evaporated and retained by the air as vapor. This difference between 0% supersaturation of ice and supercooled water is [from Eq. (24)] peaked at about 0.2 (g/m^3) between -10 and -20 °C and falls off at colder temperatures. This result is consistent with the fact that Eq. (24) has an e-folding length of about 15 °C.

While this may appear to be an efficient way to clear an ice crystal cloud, one must consider the timescale for the evaporation of a liquid spherical drop formed from a melted ice crystal suspended in air at 0% supersaturation

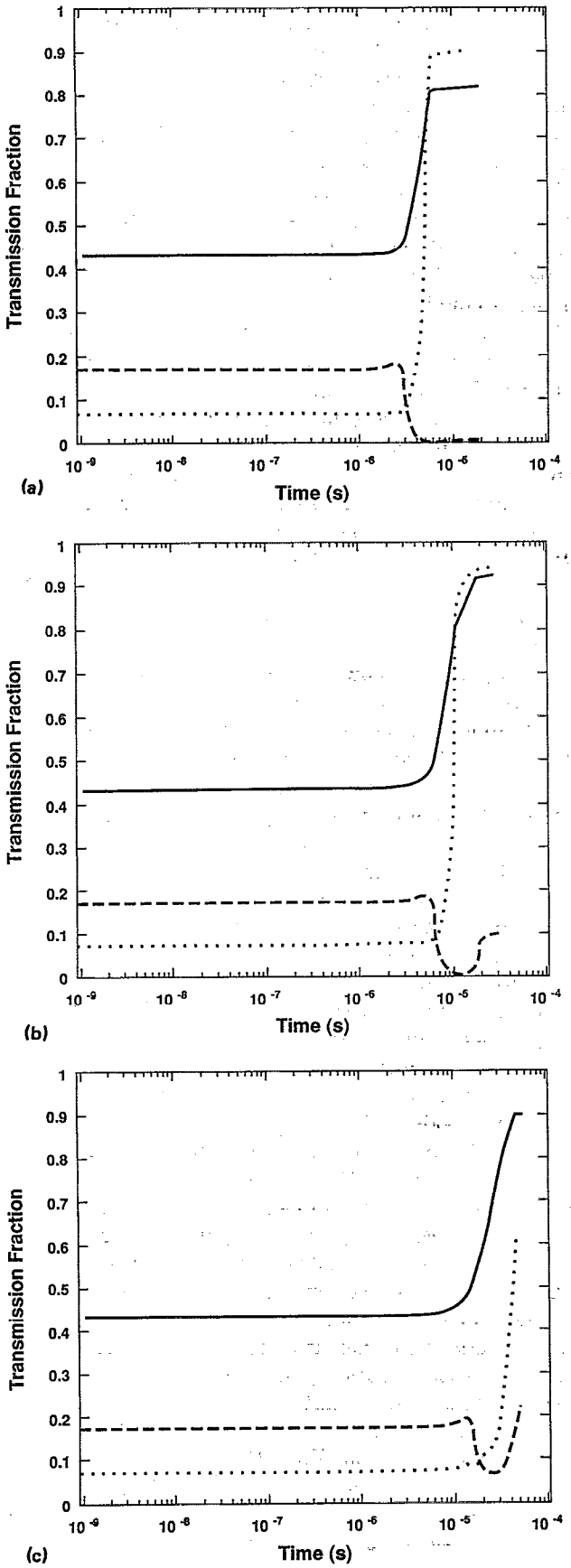

FIG. 9. Transmission fraction vs time: 10.6 μm (solid curve), 3.8 μm (dotted curve), 1.06 μm (dashed curve). (a) 0.5 MW/cm^2, 3-J/cm^2 pulse. (b) 0.25 MW/cm^2, 5-J/cm^2 pulse. (c) 0.1 MW/cm^2, 5-J/cm^2 pulse.

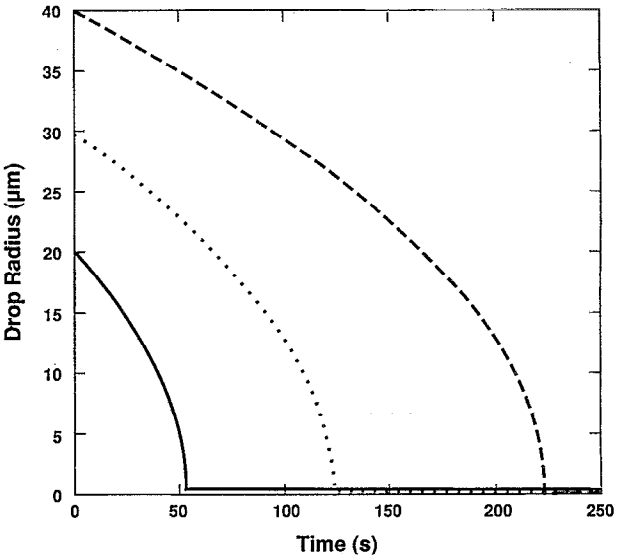

FIG. 10. Drop size in microns vs time for freely evaporating water drops with an air temperature of -15 °C and an air water vapor density set at 0% supersaturation with respect to ice.

with respect to ice. That is, the laser melts but does not evaporate the ice crystals, thus depositing much less energy than would be required for evaporation. Calling this timescale τ_{evap}, from Eqs. (22) and (23) we have

$$\tau_{\text{evap}} \equiv \left(\frac{1}{r_d}\frac{dr_d}{dt}\right)^{-1} \approx \frac{r^2}{D(\rho_{v\infty}-\rho_{wv})} \propto \frac{r^2 p_{\text{air}}}{T_a^{3/2}(\rho_{v\infty}-\rho_{wv})}, \tag{31}$$

where we have assumed that the liquid water drop is supercooled and at the air temperature but does not refreeze. For a 20-μm radius drop with $\rho_{v\infty}$ and ρ_{wv} set at 0% supersaturation over ice and water, respectively, at -15 °C ambient air temperature and $p_{\text{air}} = 0.75$ atm, we find $\tau_{\text{evap}} \approx 40$ s. In Fig. 10 is shown the time evolution of three drop sizes, 20, 30, and, 40 μ in radius. These are of the order of the dimensions expected from melted ice crystals found in some cirrus clouds. The r^2 dependence of Eq. (31) is evident, and a 40-μm drop will take about 225 s to evaporate fully. We might reasonably decrease p_{air} by a factor of three and T_a to -30 °C. From Eq. (31) this will cause virtually no change in the result since $\rho_{v\infty} - \rho_{wv}$ will decrease by about a factor of three (from the Clausius–Clapeyron equation). Of course, much shorter evaporation times may be obtained if the ice crystals shatter into small pieces before melting occurs.

ACKNOWLEDGMENT

We wish to thank Dr. R. L. Armstrong and Dr. Bae-Sig Park for useful discussions of water drop superheating and explosion.

APPENDIX: NUMERICAL SOLUTION OF MODEL EQUATIONS

The system of Eqs. (20)–(25) that comprise the low laser flux model are all ODEs: the first in the spatial coor-

dinate z valid at every time t, the rest in time at every z. (Here, $z=0$ is always the bottom of the cloud; all quantities are in cgs units.) The first equation, which determines $I(z,t)$, is solved trivially given γ. This quantity is obtained as

$$\gamma=\sum_{i,j} N_{i,j}(\sigma_{msc(i,j)}+\sigma_{mab(i,j)})+\gamma_{\text{direct}},$$
$$\equiv\gamma_{msc}+\gamma_{mab}+\gamma_{\text{direct}}, \tag{A1}$$

where the Mie absorption and scattering cross sections $\sigma_{msc(i,j)}$ and $\sigma_{mab(i,j)}$ are found in a table of data as a function of the drop radii $r_{i,j}$; γ_{direct} is the direct air molecular absorption coefficient. Knowing $I(z,t)$, the power absorbed by a water drop of size i and type j per unit length and unit beam area at point z for a cell of size Δz is

$$P_{i,j}=\frac{\sigma_{mab(i,j)}}{\gamma_{mab}\Delta z} I(z,t)[1-\exp(-\gamma_{mab}\Delta z)], \tag{A2}$$

which enters Eq. (21) as the energy input term.

To determine the time evolution of the water drops at every position z we solve Eqs. (21)–(25) for the drop temperature, $T_{i,j}(z,t)$, and the effective water volume of a drop $\tilde{m}_{i,j}(z,t)$, defined as

$$\tilde{m}_{i,j}=r_{i,j}^3-r_{s,j}^3, \tag{A3}$$

[$\tilde{m}_{i,j}$ is a more convenient variable to use than $r_{i,j}$ due to the form of Eqs. (21)–(25) in the $r_{i,j}\to r_{s,j}$, $\tilde{m}_{i,j}\to 0$ limit.] Solving Eqs. (21)–(23) for $T_{i,j}$ and implicitly (full forward) differencing the resulting equation in time results in

$$T_{i,j}^{n+1}=\frac{\left\{T_a\kappa_a r_{i,j}+\frac{P_{i,j}}{4\pi}+\frac{c_w\rho_w\tilde{m}_{i,j}}{3\Delta t}T_{i,j}^n+DL\left[\rho_{v\infty}r_{i,j}-\rho_{\text{sat}}\left(1-\frac{LM_w}{RT_a}\right)f(a,b)\right]\right\}}{\left\{r_{i,j}\kappa_a+\frac{L^2DM_w\rho_{\text{sat}}}{RT_a^2}f(a,b)+\frac{c_w\rho_w\tilde{m}_{i,j}}{3\Delta t}\right\}}, \tag{A4}$$

where

$$f(a,b)=\frac{(r_{i,j}+a_{i,j})}{[1+(b_j r_{s,j}^3/\tilde{m}_{i,j})]}.$$

The superscripts n and $n+1$ in Eq. (A4) indicate old and new time levels respectively, where Δt is the timestep. All quantities on the right-hand side are known at level n. [Implicit differencing removes stiffness associated with rapid drop temperature rise. For large Δt Eq. (A4) gives the steady-state limit of Eqs. (21)–(25) with respect to drop temperature.] Using Eq. (A4) for $T_{i,j}$ at the advanced time level in Eqs. (22) and (23) we obtain for the time evolution of the effective drop water volume

$$\frac{d\tilde{m}_{i,j}}{dt}=\frac{3D}{\rho_w}\frac{\left\{\rho_{v\infty}\kappa_a r_{i,j}^2-\rho_{\text{sat}}f(a,b)\left(\kappa_a r_{i,j}+\frac{LM_w}{4\pi RT_a^2}P_{i,j}\right)+\frac{c_w\rho_w\tilde{m}_{i,j}}{3\Delta t}\left[\rho_{v\infty}r_{i,j}-\rho_{\text{sat}}f(a,b)\left(1-\frac{LM_w}{RT_a}\left[1-\frac{T_{i,j}^n}{T_a}\right]\right)\right]\right\}}{\left\{\kappa_a r_{i,j}+\frac{L^2DM_w\rho_{\text{sat}}f(a,b)}{RT_a^2}+\frac{c_w\rho_w\tilde{m}_{i,j}}{3\Delta t}\right\}}, \tag{A5}$$

where all quantities are as previously defined. [In the actual coding of Eqs. (A4), (A5), (A8) $r_{i,j}$ is always eliminated in favor of $\tilde{m}_{i,j}$ via Eq. (A3)!] Finally, energy and mass conservation determine T_a and $\rho_{v\infty}$ at the new time $n+1$ level as

$$T_a^{n+1}=T_a^n+c_p^{-1}\sum_{i,j}P_{i,j}N_{i,j}\Delta t+\sum_{i,j}\frac{4\pi}{3}c_p^{-1}\rho_w N_{i,j}$$
$$\times[L(\tilde{m}_{i,j}^{n+1}-\tilde{m}_{i,j}^n)-c_w\tilde{m}_{i,j}^n(T_{i,j}^{n+1}-T_{i,j}^n)]$$
$$-\frac{4\pi\rho_w M_{\text{air}}}{3M_w}\sum_{i,j}N_{i,j}(\tilde{m}_{i,j}^{n+1}$$
$$-\tilde{m}_{i,j}^n)(T_{i,j}^{n+1}-T_a)/\rho_{\text{air}}$$
$$+I(z)[1-\exp(-\gamma_{\text{direct}}\Delta z)]\Delta t/(\Delta z c_p), \tag{A6}$$

and

$$\rho_{v\infty}^{n+1}=\rho_{v\infty}^n-\frac{4\pi\rho_w}{3}\sum_{i,j}N_{i,j}(\tilde{m}_{i,j}^{n+1}-\tilde{m}_{i,j}^n), \tag{A7}$$

where c_p is the specific heat of air at constant pressure and ρ_{air} is the air mass density. In Eq. (A6) the first two sums come from integrating Eq. (21) in time and summing over all drops (the energy transfer from drops to air from thermal conduction), the next term gives the temperature equilibration of water vapor from droplet evaporation with the ambient air (this term is zero if $\tilde{m}_{i,j}^{n+1}>\tilde{m}_{i,j}^n$), and the last term is the heating due to direct air absorption.

If Eq. (A4) indicates a drop temperature at or above the boiling point of water the high laser flux model is used. This consists of solving Eqs. (1) and (2) with $T_s=T_b$ at the drop surface by assuming $T(x,t)=T_0(t)-[T_0(t)-T_b]x^{n(t)}$. Using this assumed form in Eqs.

(1) and (2) and integrating Eq. (2) over the drop radius using x and x^2 as weight functions results in equations for $r_d(t)$, $T_0(t)$, and $n(t)$ given by[14]

$$\rho_w L \frac{dr_d^2}{dt} = 2[\kappa_a(T_b - T_a) - \kappa_w n(T_0 - T_b)], \tag{A8}$$

$$\rho_w c_w \frac{de_1}{dt} = p_l - 2\frac{c_w n(T_0 - T_b)}{L r_d^2 (n+2)}[\kappa_a(T_b - T_a) - \kappa_w n(T_0 - T_b)] - \frac{2(n+1)(n+2)}{n}\frac{\kappa_w}{r_d^2} e_1, \tag{A9}$$

$$\rho_w c_w \frac{de_2}{dt} = p_l - 3\frac{c_w n(T_0 - T_b)}{L r_d^2 (n+3)}[\kappa_a(T_b - T_a) - \kappa_w n(T_0 - T_b)] - \frac{3(n+3)\kappa_w}{r_d^2} e_2, \tag{A10}$$

where

$$e_1 = \frac{n(T_0 - T_b)}{(n+2)}, \tag{A11a}$$

$$e_2 = \frac{n(T_0 - T_b)}{(n+3)}. \tag{A11b}$$

Equations (A9) and (A10) are implicitly differenced in time with respect to e_1 and e_2. If Eq. (A4) indicates an average drop temperature less than T_b Eqs. (A4) and (A5) are once again used for drop evolution. If T_0 indicates a central temperature at or above 305 °C drops are exploded by the prescription already discussed in the main text.

To complete one timestep of size Δt we solve Eq. (20) in z; then, at all points in z we advance in time for all i and j either the low or high laser flux model equations previously given. Once we have estimates of all variables at the advanced time level we repeat the sequence using time-centered values of the coefficients $P_{i,j}$, T_a, ρ_{sat}, and $\rho_{v\infty}$. Thus, the overall predictor-corrector scheme is second order accurate in time; the operations are fully vectorized in z. The size of Δt is dynamically adjusted for accuracy by appropriately monitoring the vaporization/recondensation rates and the specified starting times of the laser pulses. Smaller time steps are needed when the laser is on. The resolution in z is set at the beginning of a run by specifying the desired number of spatial cells per e-folding of the bleaching beam. Given the cloud thickness and drop distribution as a function of z, this determines the number of uniformly spaced grid points.

[1] H. C. Van De Hulse, *Light Scattering by Small Particles* (Wiley, New York, 1957).
[2] P. S. Ray, Appl. Opt. **8**, 1836 (1972).
[3] F. Williams, Int. J. Heat Mass Transfer **8**, 575 (1965).
[4] L. D. Landau and E. M. Lifshitz, *Fluid Mechanics* (Pergamon, New York, 1982).
[5] B. S. Park and R. L. Armstrong, Appl. Opt. **28**, 3671 (1989).
[6] W. Kauzmann, *Kinetic Theory of Gases* (W. A. Benjamin, Inc., City, 1966), p. 38.
[7] V. E. Zuev, *Laser Beams in the Atmosphere* (Consultants Bureau, New York, 1982), pp. 279–282.
[8] Y. N. Grachev and G. M. Strelkov, Sov. J. Quant. Electron. **4**, 1221 (1975).
[9] N. H. Fletcher, *The Physics of Rain Clouds* (Cambridge University Press, Cambridge, MA, 1962).
[10] Y. S. Sedunov, *Physics of Drop Formation in the Atmosphere* (*Keter Publishing, Jerusalem LTD*, 1974).
[11] L. Dufour and R. Defay, "Thermodynamics of Clouds," *International Geophysics Series* (Academic, New York, 1963), Vol. 6.
[12] H. R. Pruppacher and J. D. Klett, *Microphysics of Clouds and Precipitation* (Reidel, Dordrecht, Holland, 1978).
[13] S. Twomey and J. Warner, J. Atm. Sci. **24**, 702 (1967).
[14] E. J. Caramana and R. B. Webster, J. Comp. Phys. (to be published).
[15] N. Fukuta and V. K. Saxena, J. Atmos. Sci. **30**, 1638 (1973).
[16] E. J. Caramana and R. L. Morse, Los Alamos National Laboratory Report LAUR 88-39-84.
[17] G. P. Quigley, R. B. Webster, E. J. Caramana, R. L. Morse, and G. W. York, Appl. Opt. **30**, 3041 (1991).
[18] E. J. McCartney, *Optics of the Atmosphere* (Wiley, New York, 1976), p. 248.
[19] A. P. Waggoner and L. F. Radke, Appl. Opt. **28**, 3039 (1989).